Estimates of Ion and Electron Heating Rates Extended to the Near-Sun Environment

Cole Meyer

Advised by Dr. R Bandyopadhyay & Dr. D. McComas

A Junior Paper

Submitted to the Department of Astrophysical Sciences

in Partial Fulfillment of the Requirements for

the Degree of Bachelor of Arts

Princeton University

Fall 2022

Abstract

Strong coupling between kinetic processes in the solar corona makes identifying dominant heating and acceleration mechanisms very difficult. Probing the fast solar wind in the near-Sun environment can maximize the temperature, density, and outflow speed anisotropies between protons and electrons that are key to better understanding such processes. Parker Solar Probe (*PSP*) data from its first ten encounters spanning 0.063 and 0.25 AU have been used to estimate ion and electron heating rates. These estimates extend the earlier analyses of *Helios* and *Ulysses* data to the near-Sun environment. The empirically derived volumetric proton and electron heating rates illustrate a strong dependence upon electron heat conduction across all distances, contrary to previous predictions based on only *Helios* and *Ulysses* data. This dependence alters the proton heating rate to total heating rate ratio significantly, implying that proton heating becomes *increasingly dominant* over electron heating with decreasing heliocentric distances between 0.063 and 0.3 AU.

This paper represents my work in accordance with University regulations.
/s/ Cole Meyer

Contents

1 Solar Wind Acceleration and Coronal Heating

Solar corpuscular radiation, or the solar wind, is a stream of charged particles (mostly electrons, protons, and alpha particles) accelerated away from the Sun by both the hydrodynamic pressure gradient between the hot, 10^6 K corona and interstellar space, and magnetohydrodynamic (MHD) wave pressure [13].

1.1 Hydrostatic Equilibrium

Parker [53] showed with elegance in 1958 that the atmosphere of a star such as the Sun cannot be in hydrostatic equilibrium to infinity, and therefore that the solar wind is likely mostly generated by the resulting pressure gradient. His model of the problem was the following.

We begin by assuming that this expanding gas is fully ionized, giving the total gas pressure $P(r) = 2kT(r)n(r)$, where $n(r)$ is the number density of ionized hydrogen atoms. For hydrostatic equilibrium, we use

$$\frac{d}{dr}(T(r)n(r)) = -\frac{GM_{\odot}m}{2k} \cdot \frac{n(r)}{r^2} \tag{1}$$

where m is the mass of a hydrogen atom. Both ionized and neutral hydrogen have thermal conductivities of [11]

$$\kappa(T) = \beta T^{\gamma} \tag{2}$$

where γ and β are positive constants. Then, we find that the steady-state heat-flow equation, $\nabla \cdot (\kappa(T)\nabla T) = 0$, yields

$$T(r) = T_0 \left(\frac{a}{r}\right)^{1/(\gamma+1)} \tag{3}$$

where a is the radius beyond which there are no sources of coronal heating. Given $T(r)$, we can integrate Equation 1 to find that

$$n(r) = n_0 \left(\frac{r}{a}\right)^{1/(\gamma+1)} \exp\left\{\left[\frac{\lambda(\gamma+1)}{\gamma}\right]\left[\left(\frac{a}{r}\right)^{\gamma/(\gamma+1)} - 1\right]\right\} \tag{4}$$

where γ is the dimensionless parameter $GM_{\odot}m/2kT_0a$. Since $P(r) = 2kT(r)n(r)$,

$$P(r) = P_0 \exp\left\{\left[\frac{\lambda(\gamma+1)}{\gamma}\right]\left[\left(\frac{a}{r}\right)^{\gamma/(\gamma+1)} - 1\right]\right\} \tag{5}$$

$$P(\infty) = P_0 \exp\left\{\left[-\frac{\lambda(\gamma+1)}{\gamma}\right]\right\} \tag{6}$$

For ionized hydrogen, we have $n = 2.5$, $a = 10^6$ km, $T_0 = 1.5 \times 10^6$ K, and $M_\odot = 1.99 \times 10^{30}$ kg, yielding $\lambda = 5.36$ and $P(\infty) = 0.55 \times 10^{-3}\ P_0$. For un-ionized hydrogen we have $n = 0.5$, which yields $P(\infty) = 10^{-7}\ P_0$. P_0 is defined as $P_0 = P(a)$, and Parker estimated that $n_0 = 3 \times 10^7 \text{cm}^{-3}$ and $T_0 = 1.5 \times 10^6$K, so $P_0 = 1.3 \times 10^{-2}$ dynes cm^{-2}. Therefore, even after subtracting the interstellar gas pressure (Parker estimates 10 hydrogen atoms per cm^3 at 100 K, giving 1.4×10^{-13}dynes cm^{-2}), there exists a non-vanishing hydrodynamic pressure at infinity. Parker concluded that a simple static corona was not a viable possibility [17].

After turning to the momentum equation for steady radial outflow to remedy this conflict, Parker [52] showed that the solution most consistent with observation transitioned from quasi-static near the Sun to supersonic at large heliocentric distances via a *hydrodynamically expanding corona*.

1.2 Missing Pressure Gradient

While Parker's hydrodynamically expanding corona was confirmed in part shortly after its proposal by the Explorer 10 [4, 5, 59], and Mariner 2 [50, 51] spacecraft, his theory did not explain how particles are accelerated or where the particles are accelerated from in order to form the solar wind [44]. There must be some additional pressure gradient to enable the observed solar wind acceleration.

1.2.1 Direct Acceleration by Magnetic Pressure Gradient

There have been studies showing the influence of direct acceleration by the gradient of magnetic pressure associated with the radial decrease in Alfvén wave amplitude [1, 15, 16, 34, 45, 47, 66]. It has been shown that Alfvén wave pressure is relatively important to solar wind acceleration when the Alfvén wave energy is important compared to thermal energy (for low coronal temperatures) [1, 15], and that wave dissipation (detailed in section 1.2.2) alone is insufficient to drive high-speed streams [28, 34].

1.2.2 Heating by Dissipation

Others have reframed the solar wind acceleration problem as one of coronal heating. If we can identify the mechanism which *energizes* the solar wind, perhaps we can then deduce how the solar wind is actually accelerated and heated.

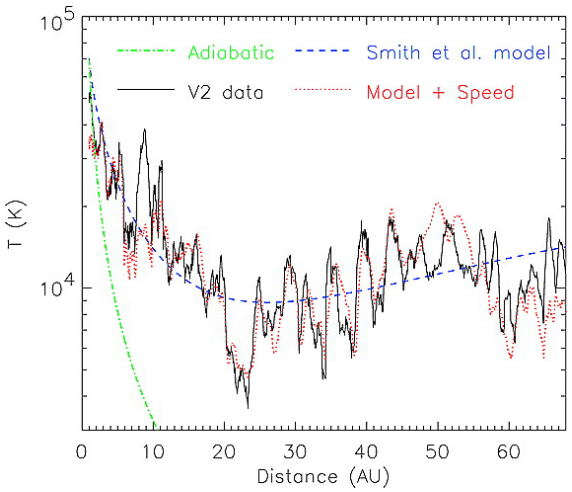

Fig. 1: Running boxcar averages of *Voyager 2* temperature data (solid line) and the adiabatic profile (dot-dash line) versus radial distance, reproduced from Richardson et al. [57].

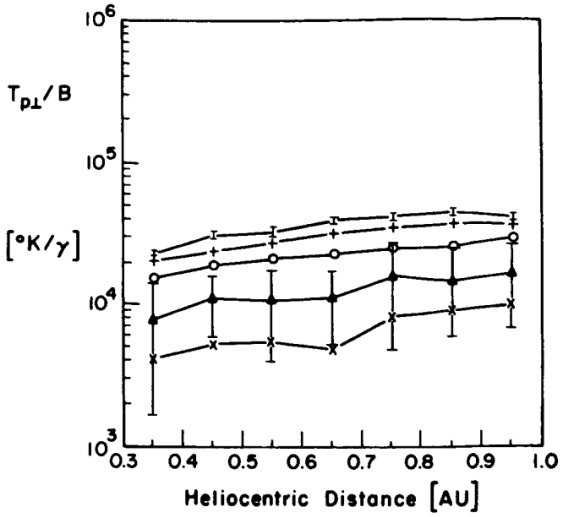

Fig. 2: Proton magnetic moment versus heliocentric distance for various solar wind velocities, derived from *Helios* data, reproduced from Marsch et al. [41].

It has been established that the heating mechanism of interest likely requires extremely large and anisotropic coronal temperatures [44]. The adiabatic (Q=0) expansion law has that $T(r) \propto r^{-\gamma}$ for $\gamma = 4/3$, but several studies have shown non-adiabaticity in the solar wind via significantly lower values of $\gamma \in [0.7,1]$ in the mean radial trends of proton temperature [9, 21, 36, 39–41, 57, 60, 61], suggesting additional extended heat deposition into the corona. This can be seen clearly in the raw mean radial trends (see Fig. 1), as well as in the radial dependency of the proton magnetic moment, which we would expect to remain constant for a collisionless double adiabatic plasma (see Fig. 2) [41].

Several potential heating mechanisms have been proposed, but the focus of this paper will be on the dissipation of magnetohydrodynamic (MHD) waves via mechanisms like phase mixing [24] or resonant absorption [27]. Of the various flavors of MHD waves, low-frequency Alfvén waves are a strong candidate for their ability to transfer energy efficiently across large distances while surviving the sharp gradients of the solar transition region, thereby enabling the transfer of energy from the photosphere and chromosphere to the corona [44], but our analyses will apply to MHD dissipative mechanisms generally.

1.3 Probing Kinetic Processes

The various particle species of the mainly collisionless solar wind (e.g., protons, electrons, and alpha particles) are not in thermal equilibrium with one another; they exhibit different outflow speeds, temperatures, and velocity distributions (see Fig. 3) [37]. In the fast solar

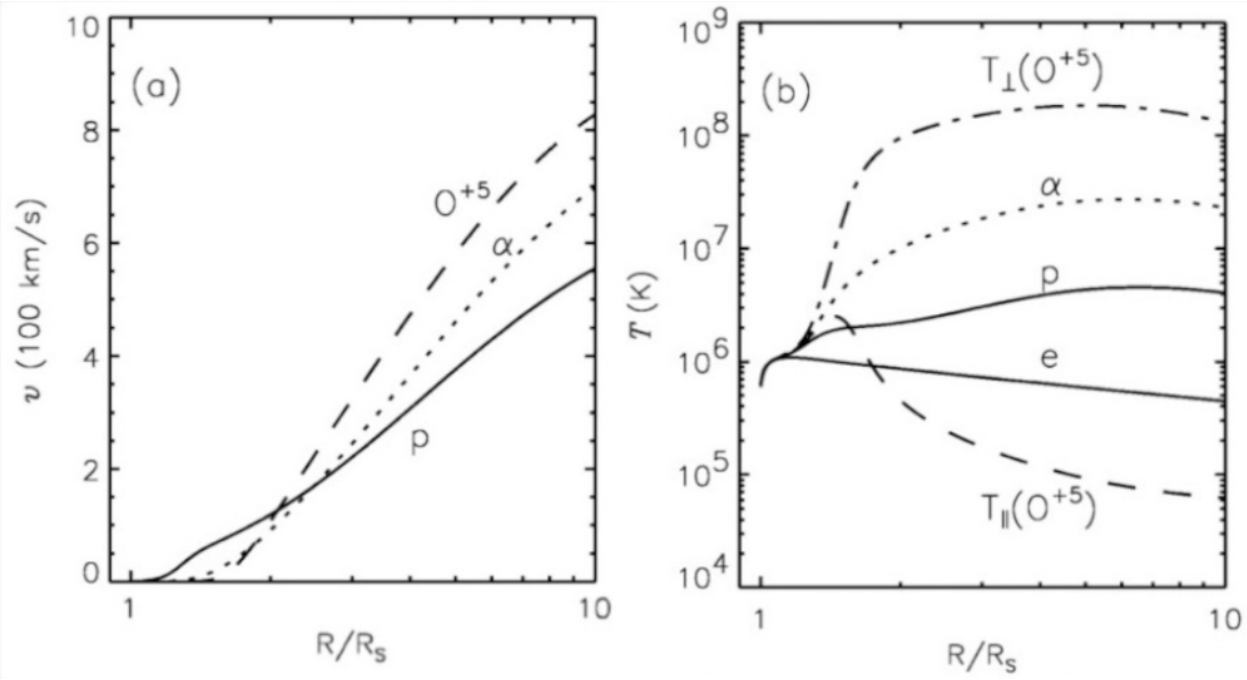

Fig. 3: Multifluid solar wind model computations for electron/protons, alpha particles, and oxygen ions: (a) flow speeds and (b) temperature of species, reproduced from Li et al. [37].

wind (where there are fewer Coulomb collisions than the slow wind), the anisotropies are even more pronounced [2, 13, 32, 33, 48].

These kinetic properties can be used to probe processes like the dissipation of MHD waves and others like fast and slow magneto-sonic wave modes, joule heating, and nano-flares. Therefore, effective study of kinetic processes in the corona – and by extension, coronal heating and acceleration mechanisms – relies crucially on the fast solar wind. Past studies have used these anisotropies to derive heating rates from various mechanisms [8, 12, 20, 38, 39, 43, 64, 67–69].

1.4 Previous Work

Previous studies have made similar estimates of the rates of energy input into the solar wind, but many of them have either treated protons or electrons independently [55, 56, 63] or treated one independently and inferred the other [35, 65]. A complete treatment requires an equal consideration of both proton and electron heating rates, especially considering their comparable thermal energy contributions.

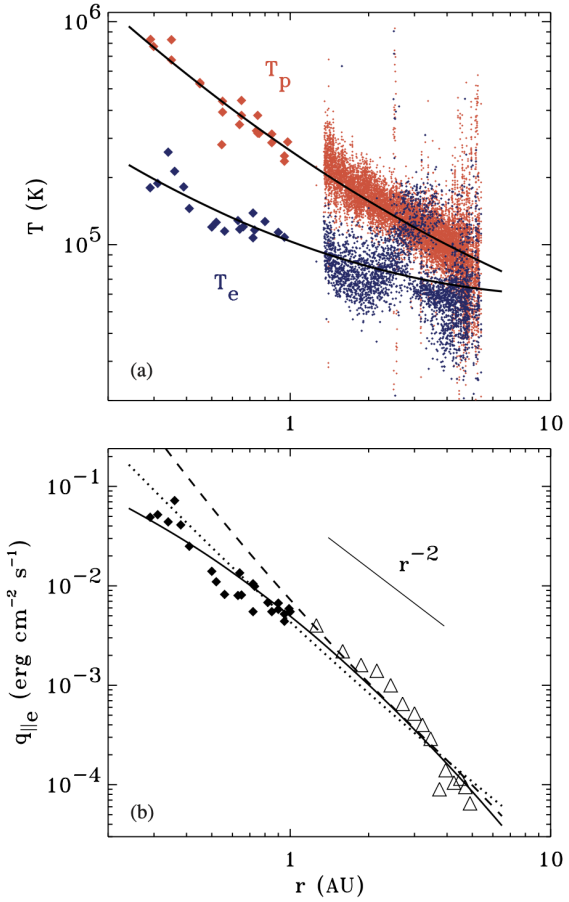

Fig. 4: In situ measurements for the fast solar wind: (a) plasma temperatures from *Helios* (filled diamonds) and *Ulysses* (small points), with protons in red and electrons in blue. (b) Electron heat conduction flux from *Helios* (filled diamonds) and *Ulysses* (triangles). Also shown are least-squares fits (solid lines), the classical Spitzer-Härm heat flux (dashed line), and the Hollweg [25, 26] collisionless heat flux with $\alpha_e = 1.05$ (dotted line), reproduced from Cranmer et al. [13].

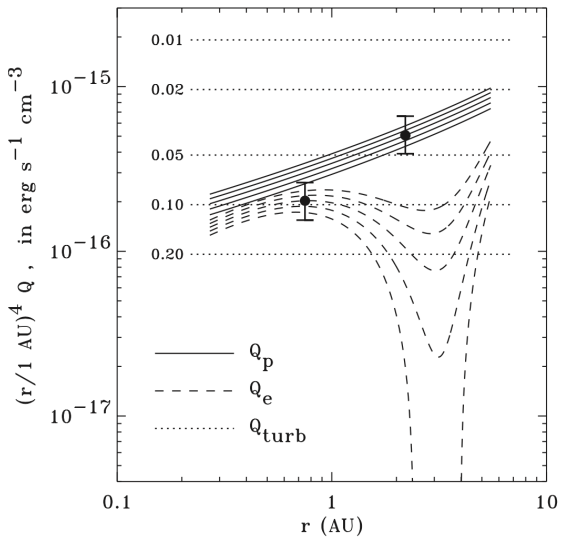

Fig. 5: Empirically derived heating rates for protons (solid lines) and electrons (dashed lines) in the fast solar wind, with multiple curves showing results for u = 600, 650, 700, 750, and 800 km s^{-1} (from bottom to top for each set of curves). Shown for comparison is Q_{turb} for five values of $\lambda_\perp$ at 1 AU (dotted lines). All heating rates have been multiplied by (r/1 AU)^4. Example error bars are given for the u = 700 km s^{-1} case, reproduced from Cranmer et al. [13].

Cranmer et al. [13] performed a complete treatment of this type, and will serve as a model for the subsequent paper. They used only fast solar wind data (u > 600 km s^{-1}) to derive the following analytic fits for proton temperature, electron temperature, and electron heat conduction flux (see Fig. 4):

$$\ln\left(\frac{T_p}{10^5\mathrm{K}}\right) = 0.9711 - 0.7988x + 0.07062x^2 \tag{7}$$

$$\ln\left(\frac{T_e}{10^5\mathrm{K}}\right) = 0.03460 - 0.4333x + 0.08383x^2 \tag{8}$$

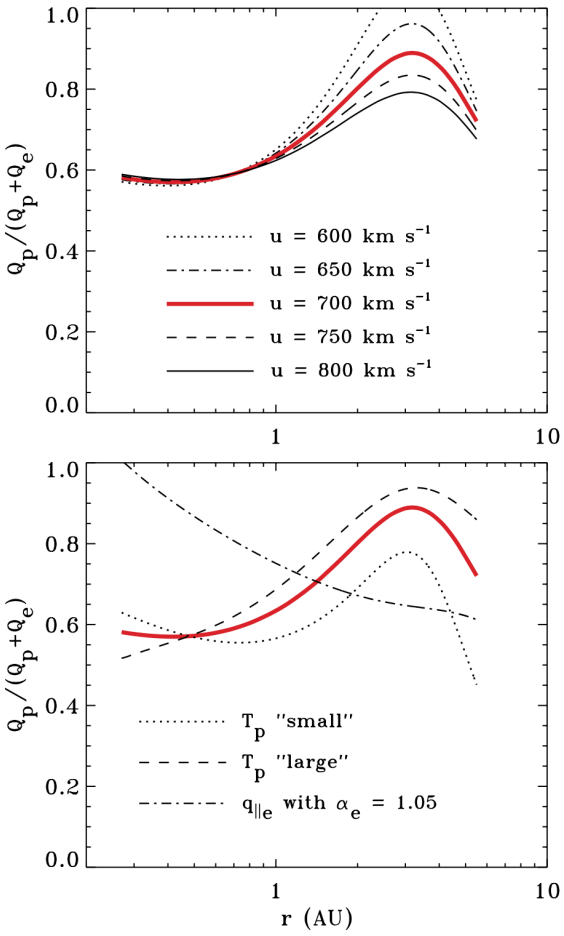

Fig. 6: Ratios of the proton heating rate to the total (proton + electron) heating rate. The standard model with wind speed u = 700 km s^{-1} is shown in both panels (thick red line). (a) Variation of the wind speed between 600 and 800 km s^{-1} in 50 km s^{-1} increments (see labels). (b) Models computed with T_{small} (dotted line) and T_{large} (dashed line) limiting cases for the SWOOPS proton temperatures, and the Hollweg [25, 26] collisionless heat flux instead of the empirical fit (dot-dashed line), reproduced from Cranmer et al. [13].

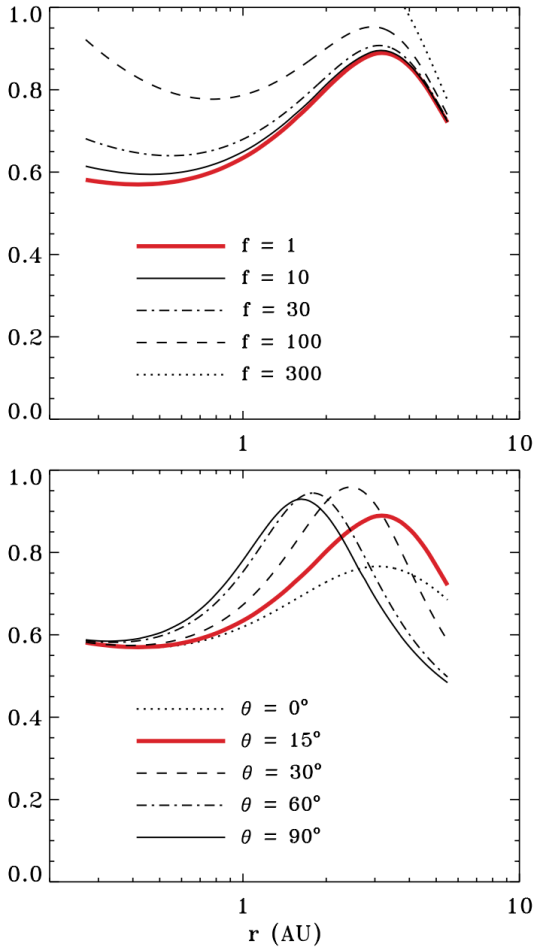

Fig. 7: Same as Figure 7, but with other parameters varied. (a) A series of models with anomalously strong Coulomb collisions, with a range of constant multipliers f to the classical collision frequency (see labels). (b) Models computed over a range of colatitudes θ in the heliosphere, which affects the Parker spiral angle Φ. The standard model with wind speed u = 700 km s^{-1} is shown in both panels (thick red line), reproduced from Cranmer et al. [13].

$$\ln\left(\frac{q_{||,e}}{q_0}\right) = -0.7032 - 2.115x + 0.2545x^2 \qquad (9)$$

where $x \equiv \ln(\mathrm{r}/[1\ \mathrm{AU}])$ and $q_0 = 0.01$ erg cm^{-2} s^{-1}. Cranmer et al. numerically differentiated these values using the standard centered-difference approximation and derived the corresponding proton and electron heating rates (details of this specific method will be developed in section 3). These heating rates have been reproduced in Fig. 5, Fig. 6, and Fig. 7. Notably, they conclude that protons receive 60% of the total plasma heating in

the inner heliosphere, and that the fraction increases to 80% of the total by the orbit of Jupiter. A more thorough review of their results will follow.

1.5 Parker Solar Probe and the Near-Sun Environment

As the solar wind propagates outward, it is increasingly slowed and heated by the ionization of neutral interstellar pickup ions, and the heating mechanisms which once drove its acceleration become less impactful. These effects serve to erase information about those energization mechanisms that the solar wind might hold in the near-Sun environment. If we wish to study solar wind acceleration and the mechanisms that drive it, we must investigate the near-Sun environment, where those propagation effects are minimized and acceleration is ongoing [18, 31].

The Parker Solar Probe (*PSP*) provides data from the near-Sun environment with the goals of (1) tracing the flow of energy that heats the solar corona and accelerates the solar wind, (2) determining the structure and dynamics of the plasma and magnetic fields at the sources of the solar wind, and (3) exploring the physical mechanisms that produce, accelerate, and transport energetic particles in the inner heliosphere [31]. PSP will make 24 encounters with the Sun between August 2018 and August 2025, spanning heliocentric distances of 0.046 AU and 0.25 AU (see Fig. 8).

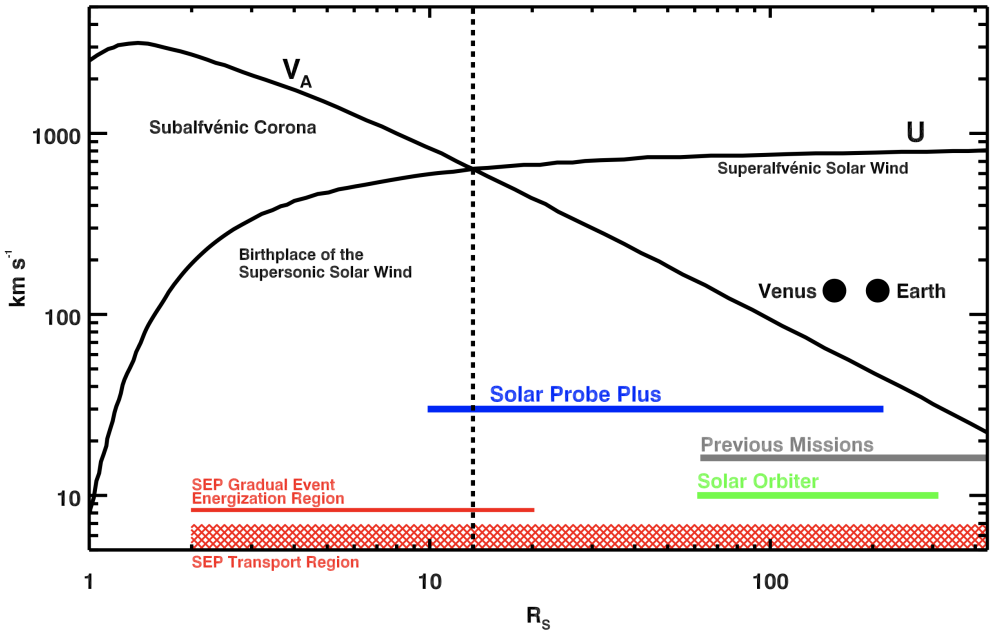

Fig. 8: Model profiles of solar wind speed U and Alfvén wave speed V_A versus helioradius. The *vertical bar* separates the source, or sub-Alfvénic, region of the wind from the super-Alfvénic solar wind flow. Orbital range for *Solar Probe Plus* (renamed to *Parker Solar Probe*), *Solar Orbiter*, and other previous missions [19].

2 In Situ Plasma Measurements

We collect and analyze *PSP*, *Helios*, and *Ulysses* data from the fast solar wind at heliocentric distances of 0.063 – 0.25 AU for *PSP*, 0.30 – 0.98 AU for *Helios*, and 1.26 – 5.44 AU for *Ulysses*: 0.063 – 5.44 AU in combination.

2.1 Parker Solar Probe Data

Onboard PSP are four suites of instruments designed to take *in situ* electric and magnetic field measurements, as well as measurements of the solar wind plasma its energetic particles: FIELDS (electromagnetic fields), SWEAP (solar wind plasma), IS⊙IS (energetic particles), and WISPR (coronal structure imaging) [31].

SWEAP [29], a four sensor instrument suite designed to provide measurements of the electrons and ionized helium and hydrogen which constitute the solar wind and coronal plasma, will provide our proton temperature T_p and outflow speed u data. SWEAP is comprised of the Solar Probe Cup (SPC) [10], a Faraday Cup that measures ion and electron fluxes and flow angles as a function of energy, and the Solar Probe ANalyzers (SPAN) [70], which measures the ion composition and three-dimensional distribution function of the corona. We utilized the moments from SPC (as opposed to the fits) to avoid assuming Maxwellian ion distributions. Proton temperature was calculated from the given proton thermal speed moment v_{th} using the standard $v_{th} = \sqrt{2kT/m}$, where m is proton mass. SPAN-I did not resolve the full velocity distribution function (VDF) very well during the first three encounters, and SPC did not observe the core solar wind very well after encounter 4 while SPAN-I was able to resolve the VDF from encounter 4 onwards, so we have utilized SPC data for the first three encounters and SPAN-I data for the last seven encounters [54].

FIELDS [3, 46], a suite of instruments designed to measure magnetic and electric fields, plasma wave spectra, and solar radio emissions, will provide our electron heat conduction flux $q_{||,e}$, electron temperature T_e, and electron density n_e data. The suite returned poor data for encounter three, so we will omit them from our analyses.

The following work will make use of data from the first 10 encounters from *PSP* (0.063 AU to 0.25 AU), a dramatic improvement upon similar work in the past, most of which make use of encounters 1 and 2.

2.2 Helios and Ulysses Data

All *Helios* and *Ulysses* data were taken from Cranmer et al. [13], who collected the data from various sources: Helios proton temperatures from Marsch et al. [41], Helios electron temperature and heat conduction flux from Pilipp et al. [56], and Ulysses electron heat conduction flux from Scime et al. [62]. Their Ulysses proton and electron temperature data was collected directly from the European Space Agency's online archive [13]. Note that the Ulysses heat conduction flux data was not filtered for winds at outflow speeds greater than 600 km s^{-1} and that the Ulysses electron temperature data shows a noticeable bifurcation around $r \approx 3$–4 AU, which Cranmer et al. attributes to a solar cycle effect. It is possible that this bifurcation has affected the subsequent electron temperature fit, and will be further discussed in section 3.

We do not have proton or electron density data from *Helios* or *Ulysses* from the Cranmer et al. study [13], so we will return the assumption from Cranmer et al. [13] that both n_p and n_e are proportional to r^{-2} and that n_p is normalized to 2.5 cm^{-3} at 1 AU for the *Helios* and *Ulysses* distance ranges [13, 22]. We will also utilize the assumption of 5% helium abundance to find that $n_e = 1.1\ n_p$ and calculate n_p indirectly for all three datasets, given the relatively accuracy of n_e and n_p measurements from *PSP* and the absence of density data from *Helios* and *Ulysses*.

We define the fast solar wind to be streams faster than 600 km s^{-1} for all three datasets. While higher than the standard velocity cutoff of 500 km s^{-1} for the fast solar wind, our cutoff helps to minimize contamination from the slow solar wind, which carries different properties than the fast wind [13, 14, 38]. We do not have velocity data from *Helios* or *Ulysses*, but *PSP* yields a mean velocity of 651 km s^{-1} with a standard deviation of 51 km s^{-1} after applying a velocity cutoff of 600 km s^{-1}. Cranmer et al. [13] reports a mean velocity of 744 km s^{-1} with a standard deviation of 47 km s^{-1} after applying the same velocity cutoff to the *Helios* and *Ulysses*.

2.3 Complete Analytic Fits

Fig. 9 shows the following analytic fits from the combined *PSP*, *Helios*, and *Ulysses* datasets between 0.063 and 5.44 AU:

$$\ln\left(\frac{T_p}{10^5\mathrm{K}}\right) = 0.9988 - 0.6576x + 0.0423x^2 \tag{10}$$

$$\ln\left(\frac{T_e}{10^5\mathrm{K}}\right) = 0.0957 - 0.3776x + 0.1376x^2 \tag{11}$$

$$\ln\left(\frac{q_{||,e}}{q_0}\right) = -0.7752 - 2.4069x - 0.0574x^2 \tag{12}$$

where $x \equiv \ln(\mathrm{r}/[1\ \mathrm{AU}])$ and q_0 =0.01 erg cm^{-2} s^{-1}. We have assumed that the electron density can be well approximated by a power law fit, but have not assumed anything about the values of that fit:

$$n_e = 3.064 \times r^{-2.173} \tag{13}$$

To equally weight each dataset during the fitting process, we have binned and averaged the combined datasets into 100 bins, thereby erasing any non-uniformity in the number of data points between the three. The fits were then found based on the resulting 100 data points.

We observe slightly different concavities between our temperature fits and those from Cranmer et al. [13], as well as the likely presence of an electron temperature "shelf" beyond 1 AU as predicted by Breech et al. [7], but more noticeably, dramatically flatter fits in the electron heat conduction flux data. We can compare these fits with those of Cranmer et al. more readily by calculating their respective power-law dependencies according to

$$\delta = -\frac{\partial \ln(q_{||,e})}{\partial \ln(r)} \rightarrow q_{||,e} \propto r^{-\delta} \tag{14}$$

We find that the fit from Cranmer et al. yields δ approximately equal to 2.12 at 1 AU which drops to 0.94 at 0.1 AU, while our fit holds relatively constant with 2.52 at 1 AU and 2.41 at 0.1 AU. This continuous heat conduction flux contribution implies more outward heat conduction than would be expected from the fits of Cranmer et al. Therefore, we expect that our electron heating rate will be lower than that from Cranmer et al. in the inner heliosphere [13].

3 MHD Turbulence Heating Rates

We have employed the same internal energy conservation equations as Cranmer et al. [13]. These equations attempt to calculate the rates of heating and cooling for as many known physical processes as possible – including adiabatic energy conservation, electron heat conduction, and Coulomb collisions – and derive the corresponding net volumetric heating rates, presumably due to MHD turbulence [13].

We have neglected temperature anisotropies as contributions to net heating because they've been shown to affect the net heating only negligibly [41, 42, 56, 68] and tend to return to isotropy as a result of plasma instabilities [23, 30]. We have also neglected proton heat conduction because the contribution from electron heat conduction is much larger [6, 13, 58]

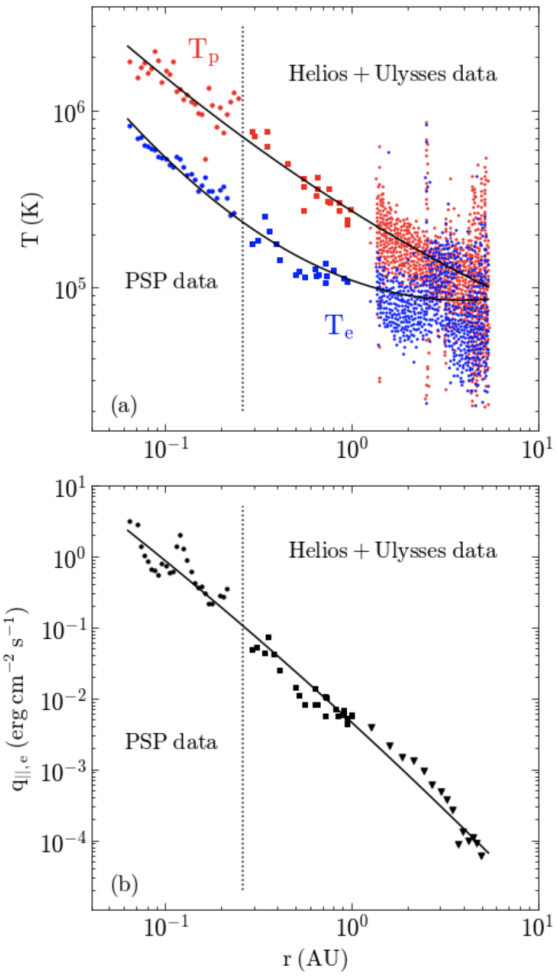

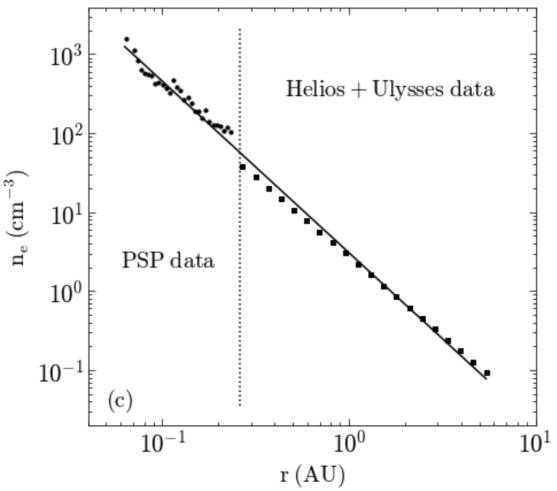

Fig. 9: *In situ* measurements of the fast solar wind: (a) proton and electron temperature from *PSP* (filled stars), *Helios* (filled squares), and *Ulysses* (small points) with protons in red and electrons in blue. (b) electron heat conduction flux from *PSP* (filled stars), *Helios* (filled squares), and *Ulysses* (small points). (c) electron density from *PSP* (filled stars). In all plots, analytic fits of the combined datasets (solid line) are shown. Vertical dotted lines denote the separation between *PSP* data and other data.

3.1 Internal Energy Conservation Equations

Given those choices, we have the following proton and electron internal energy conservation equations [13]:

$$Q_p = \frac{3}{2} n_p u k_B \frac{\partial T_p}{\partial r} - u k_B T_p \frac{\partial n_p}{\partial r} + \frac{3}{2} n_p k_B \nu_{pe} (T_p - T_e) \tag{15}$$

$$Q_e = \frac{3}{2} n_e u k_B \frac{\partial T_e}{\partial r} - u k_B T_e \frac{\partial n_e}{\partial r} - \frac{3}{2} n_e k_B \nu_{ep} (T_p - T_e) + \frac{1}{r^2} \frac{\partial}{\partial r} (q_{||,e} r^2 \cos^2 \Phi) \tag{16}$$

where the volumetric heating rates are Q_p and Q_e. We also have proton-electron collisions of ν_{pe} and ν_{ep} and have assumed a constant outflow speed u of 700 km s^{-1}. The Parker spiral angle is Φ, given in its standard form as

$$\tan\Phi = \Omega\, r \sin\theta / u \tag{17}$$

with a rotation frequency of $\Omega = 2.7$ x 10^{-6} rad s^{-1} and a colatitude of $\theta = 15°$. We have utilized the proton-electron collision rate scaling relations given by Cranmer et al. [13]

$$\nu_{pe} \approx 8.4 \times 10^{-9} \left(\frac{n_e}{2.5 \text{ cm}^{-3}}\right) \left(\frac{T_e}{10^5 \text{ K}}\right)^{-3/2} \text{s}^{-1} \tag{18}$$

$$\nu_{ep} \approx 8.4 \times 10^{-9} \left(\frac{n_p}{2.5 \text{ cm}^{-3}}\right) \left(\frac{T_p}{10^5 \text{ K}}\right)^{-3/2} \text{s}^{-1} \tag{19}$$

We numerically computed each derivative based on the fits in Equations 10, 11, and 12 using the standard centered-difference approximation on a very fine grid of 1000 points between 0.063 and 5.44 AU.

3.2 Empirically Derived Heating Rates

Fig. 10 shows the resulting heating rates. To estimate the error envelopes corresponding to each heating rate, we have extremized the proton and electron heating rates which result from multiplying T_p, T_e, $q_{||,e}$ by $(1+\sigma)^n$, where $n = -1, 0, 1$ and σ is the relative standard deviation of the respective residuals. We found that $\sigma_{T_p} = 0.14$, $\sigma_{T_e} = 0.18$, and $\sigma_{q_{||,e}} = 0.38$. To propagate those envelopes to total heat and proton heat to total heat ratios, we have performed the same procedure, varying proton and electron heat.

We found that the proton temperature is well described by the following power-law fit, consistent with Cranmer et al., valid within 23% relative accuracy across all distances:

$$Q_p = 6.05 \times 10^{-16} \left(\frac{r}{1 \text{ AU}}\right)^{-3.71} \left(\frac{u}{700 \text{ km s}^{-1}}\right) \text{erg s}^{-1} \text{ cm}^{-3} \tag{20}$$

This can be compared with the fit that Cranmer et al. found with only the *Helios* and *Ulysses* data, valid within around 6% relative accuracy:

$$Q_p = 3.42 \times 10^{-16} \left(\frac{r}{1 \text{ AU}}\right)^{-3.5} \left(\frac{u}{700 \text{ km s}^{-1}}\right) \text{erg s}^{-1} \text{ cm}^{-3} \tag{21}$$

We observe that our fits are approximately twice as large as those from Cranmer et al. at 1 AU but that they are approximately proportional to each other. Our scaling relation is comparable to the rate predicted by Verma et al. [69] for Alfvénic streams of $Q_p \propto r^{-3.3}$.

The characteristic feature of Cranmer's electron heating rates is the dominant non-local heat conduction behavior around 2 AU due primarily to the large concavity in the electron heat conduction flux fits (see Fig. 4).

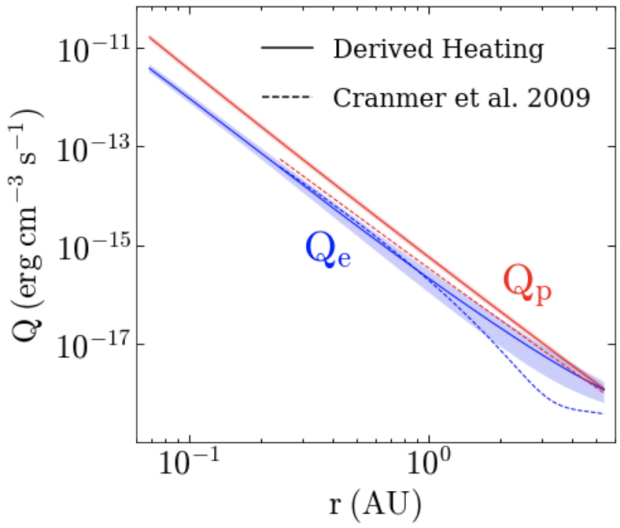

Fig. 10: Empirically derived heating rates vs. heliocentric distance. Also shown are the error envelopes described in the text.

The extended range of distances provided by *PSP* shows that their fit is *not consistent* with the full range of distances. The resulting effect is the suppression of this non-local behavior, leading to a much smoother electron heating rate near 2 AU. However, while suppressed, the still present heat conduction behavior again prevents an effective power-law fit; the closest fit was only valid to around 51% relative accuracy across all distances:

$$Q_e = 2.46 \times 10^{-16} \left(\frac{r}{1\text{ AU}}\right)^{-3.34} \left(\frac{u}{700\text{ km s}^{-1}}\right) \text{erg s}^{-1}\text{ cm}^{-3} \tag{22}$$

We can also calculate the total heating rate and compare with previous results. The following fit is valid to within 37% relative accuracy (see Fig. 11):

$$Q_{tot} = 8.59 \times 10^{-16} \left(\frac{r}{1\text{ AU}}\right)^{-3.59} \left(\frac{u}{700\text{ km s}^{-1}}\right) \text{erg s}^{-1}\text{ cm}^{-3} \tag{23}$$

approximated by a power law fit $Q \propto r^{-\delta}$ with δ slightly greater than 3.59, while the implied heating rates from Bandyopadhyay et al. have δ approximately 6.3.

Perhaps most interesting is the proton heating rate Q_p to total heating rate $Q_p + Q_e$ ratio, shown in Fig. 12. We notice a departure in behavior from the decrease in proton contribution beginning at around 3 AU observed in the equivalent ratio from Cranmer et al. (see Fig. 6 and 7). This occurs because our electron heat conduction flux fit maintains a relatively constant slope for decreasing heliocentric distances, thereby providing a larger negative contribution to the total electron heating rate.

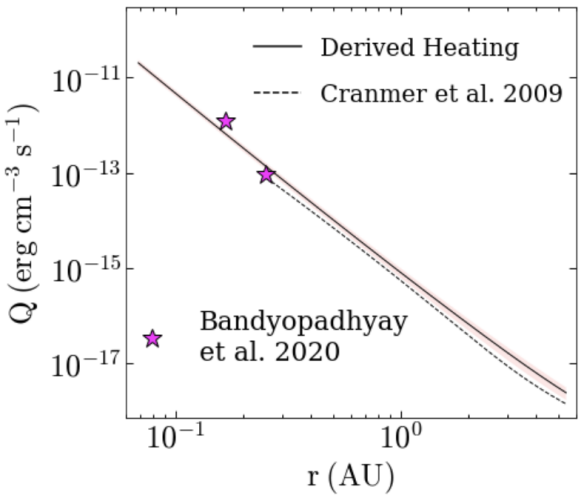

Fig. 11: Total heating rates (proton plus electron) vs. heliocentric distance. Error envelopes are described in text.

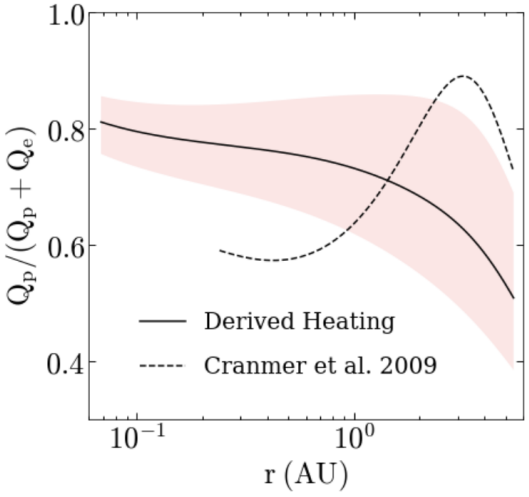

Fig. 12: Proton heating to total heating ratio vs. heliocentric distance. Error envelopes are described in text.

These limitations indicate that a significant revision in understanding from the conclusions reached by Cranmer et al. [13] is required. While the results from only *Helios* and *Ulysses* data imply a large drop in the proton contribution to the total heating rate at heliocentric distances smaller than 3 AU, *PSP* data implies the opposite: a monotonically increasing proton contribution, as well as larger proton heating rate magnitudes at heliocentric distances smaller than 5.44 AU.

4 Conclusions and Outlook

Fully understanding the validity of various heating and acceleration mechanisms in the solar corona crucially depends upon observational data from the near-Sun environment, just as the *Parker Solar Probe* provides. In this paper, we have extended the analysis of Cranmer et al. [13] by calculating volumetric proton and electron heating rates upon equal footing. We have found, contrary to the conclusions of Cranmer et al., that protons receive about 80% of the total coronal heating in the near-Sun environment and that this fraction drops to about 50% of the total heating rate by the orbit of Jupiter (around 5.2 AU).

In section 2 we described all three data sets, including the *Helios* and *Ulysses* data utilized by Cranmer et al. [13], and the *Parker Solar Probe* data we used to extend previous analyses. We applied fits to the proton and electron temperature, electron density, and electron heat conduction flux data of the combined data sets spanning 0.063 AU to 5.44 AU, and found significant differences between the full electron heat conduction flux fits and those of Cranmer et al.

In section 3 we motivated the choice of internal heat conservation equations and empirically derived the volumetric proton and electron heating rates corresponding to the full data set. Notably, we found that the flatter heat conduction flux fits resulting from the full data sets removed the majority of the non-local heat conduction around 3 AU characteristic of the electron heating rates from Cranmer et al. We also derived proton heating rate described by $Q_p \propto r^{-3.71}$, comparable to the rate predicted by Verma et al. [69] of $Q_p \propto r^{-3.3}$ and to $Q_p \propto r^{-3.5}$, as found by Cranmer et al. [13].

We await further encounters from *Parker Solar Probe*, which will help to minimize uncertainty in the raw proton and electron temperature, electron density, and electron heat conduction flux data, thereby improving the error on our derived proton and electron heating rates. Better understanding the two-fluid nature of the solar wind is key to improving our MHD dissipative heating models. In the future we hope to further compare theoretical predictions from various dissipative models with our heating rates.

Acknowledgements

The authors would like to acknowledge the invaluable contributions of Dr. Riddhi Bandyopadhyay, Associate Research Scholar at Princeton University, as well as Dr. David McComas, Professor of Astrophysical Sciences at Princeton University, for valuable discussions. In addition, they are most grateful to Paige Cromley and Ben Howe for their friendship and physical prowess. Finally, a big thank you to Katerina Kourpas for her unwavering late-night dining hall presence.

The authors thank Jasper Halekas for electron heat conduction flux data.

Parker Solar Probe was designed, built, and is now operated by the Johns Hopkins Applied Physics Laboratory as part of NASA's Living with a Star (LWS) program (contract NNN06AA01C). Support from the LWS management and technical team has played a critical role in the success of the Parker Solar Probe mission. We are deeply indebted to everyone that helped make the PSP mission possible.

The authors acknowledge CNES (Centre National d'Etudes Spatiales), CNRS (Centre National de la Recherche Scientifique), the Observatoire de PARIS, NASA, and the FIELDS/RFS team for their support to the PSP/SQTN data production, and the CDPP (Centre de Donnees de la Physique des Plasmas) for their archiving and provision.

References

[1] James Alazraki and PL Couturier. *Solar Wind Acceleration Caused by the Gradient of Alfvén Wave Pressure: Effects of Scattering on the Brightness Distribution*. Springer, 1971.

[2] E Antonucci, G Noci, JL Kohl, G Tondello, MCE Huber, S Giordano, C Benna, A Ciaravella, S Fineschi, LD Gardner, et al. First results from uvcs: Dynamics of the extended corona. In *1st Advances in Solar Physics Euroconference. Advances in Physics of Sunspots*, volume 118, page 273, 1997.

[3] SD Bale, K Goetz, PR Harvey, P Turin, JW Bonnell, T Dudok de Wit, RE Ergun, RJ MacDowall, M Pulupa, Mats André, et al. The fields instrument suite for solar probe plus. *Space science reviews*, 204(1):49–82, 2016.

[4] Charles K Birdsall and William B Bridges. Space-charge instabilities in electron diodes and plasma converters. *Journal of Applied Physics*, 32(12):2611–2618, 1961.

[5] ABRID Bonetti, HS Bridge, Alan J Lazarus, B Rossi, and F Scherb. Explorer 10 plasma measurements. *Journal of Geophysical Research*, 68(13):4017–4063, 1963.

[6] SI Braginskii and MA Leontovich. Reviews of plasma physics, 1965.

[7] Ben Breech, William H Matthaeus, SR Cranmer, JC Kasper, and Sean Oughton. Electron and proton heating by solar wind turbulence. *Journal of Geophysical Research: Space Physics*, 114(A9), 2009.

[8] Ben Breech, William H Matthaeus, J Minnie, JW Bieber, Sean Oughton, Charles W Smith, and PA Isenberg. Turbulence transport throughout the heliosphere. *Journal of Geophysical Research: Space Physics*, 113(A8), 2008.

[9] LF Burlaga and KW Ogilvie. Magnetic and thermal pressures in the solar wind. *Solar Physics*, 15(1):61–71, 1970.

[10] Anthony W Case, Justin C Kasper, Michael L Stevens, Kelly E Korreck, Kristoff Paulson, Peter Daigneau, Dave Caldwell, Mark Freeman, Thayne Henry, Brianna Klingensmith, et al. The solar probe cup on the parker solar probe. *The Astrophysical Journal Supplement Series*, 246(2):43, 2020.

[11] Sydney Chapman. The viscosity and thermal conductivity of a completely ionized gas. *The Astrophysical Journal*, 120:151, 1954.

[12] Paul J Coleman Jr. Turbulence, viscosity, and dissipation in the solar-wind plasma. *The Astrophysical Journal*, 153:371, 1968.

[13] Steven R Cranmer. Empirical constraints on proton and electron heating in the fast solar wind. *The Astrophysical Journal*, 702(2):1604, 2009.

[14] S Dasso, LJ Milano, WH Matthaeus, and CW Smith. Anisotropy in fast and slow solar wind fluctuations. *The Astrophysical Journal*, 635(2):L181, 2005.

[15] RL Dewar. Interaction between hydromagnetic waves and a time-dependent, inhomogeneous medium. *The Physics of Fluids*, 13(11):2710–2720, 1970.

[16] BR Durney and GW Pneuman. Solar-interplanetary modeling: 3-d solar wind solutions in prescribed non-radial magnetic field geometries. *Solar Physics*, 40(2):461–486, 1975.

[17] I UNIVERSAL MASS EJECTION. Mass ejection and a brief history of the solar wind concept. *Cosmic Winds and the Heliosphere*, page 3, 1997.

[18] Heather A Elliott, David J McComas, Eric J Zirnstein, Brent M Randol, Peter A Delamere, George Livadiotis, Fran Bagenal, Nathan P Barnes, S Alan Stern, Leslie A Young, et al. Slowing of the solar wind in the outer heliosphere. *The Astrophysical Journal*, 885(2):156, 2019.

[19] NJ Fox, MC Velli, SD Bale, R Decker, A Driesman, RA Howard, Justin C Kasper, J Kinnison, M Kusterer, D Lario, et al. The solar probe plus mission: humanity's first visit to our star. *Space Science Reviews*, 204(1):7–48, 2016.

[20] John W Freeman. Estimates of solar wind heating inside 0.3 au. *Geophysical research letters*, 15(1):88–91, 1988.

[21] John W Freeman and Ramon E Lopez. The cold solar wind. *Journal of Geophysical Research: Space Physics*, 90(A10):9885–9887, 1985.

[22] Melvyn L Goldstein, D_ A Roberts, and WH Matthaeus. Magnetohydrodynamic turbulence in the solar wind. *Annual review of astronomy and astrophysics*, 33:283–326, 1995.

[23] Petr Hellinger, Pavel Trávníček, Justin C Kasper, and Alan J Lazarus. Solar wind proton temperature anisotropy: Linear theory and wind/swe observations. *Geophysical research letters*, 33(9), 2006.

[24] J Heyvaerts and Eric R Priest. Coronal heating by phase-mixed shear alfvén waves. *Astronomy and Astrophysics*, 117:220–234, 1983.

[25] Joseph V Hollweg. Transverse alfvén waves in the solar wind: Arbitrary k, v 0, b 0, and— δb—. *Journal of Geophysical Research*, 79(10):1539–1541, 1974.

[26] Joseph V Hollweg. Collisionless electron heat conduction in the solar wind. *Journal of Geophysical Research*, 81(10):1649–1658, 1976.

[27] James Albert Ionson. Resonant absorption of alfvénic surface waves and the heating of solar coronal loops. *The Astrophysical Journal*, 226:650–673, 1978.

[28] SA Jacques. Solar wind models with alfvén waves. *The Astrophysical Journal*, 226:632–649, 1978.

[29] Justin C Kasper, Robert Abiad, Gerry Austin, Marianne Balat-Pichelin, Stuart D Bale, John W Belcher, Peter Berg, Henry Bergner, Matthieu Berthomier, Jay Bookbinder, et al. Solar wind electrons alphas and protons (sweap) investigation: Design of the solar wind and coronal plasma instrument suite for solar probe plus. *Space Science Reviews*, 204(1):131–186, 2016.

[30] Justin C Kasper, Alan J Lazarus, and S Peter Gary. Wind/swe observations of firehose constraint on solar wind proton temperature anisotropy. *Geophysical research letters*, 29(17):20–1, 2002.

[31] James Kinnison, Robin Vaughan, Patrick Hill, Nour Raouafi, Yanping Guo, and Nickalaus Pinkine. Parker solar probe: a mission to touch the sun. In *2020 IEEE Aerospace Conference*, pages 1–14. IEEE, 2020.

[32] JL Kohl, G Noci, E Antonucci, G Tondello, MCE Huber, SR Cranmer, L Strachan, AV Panasyuk, LD Gardner, M Romoli, et al. Uvcs/soho empirical determinations of anisotropic velocity distributions in the solar corona. *The Astrophysical Journal*, 501(1):L127, 1998.

[33] John L Kohl, Giancarlo Noci, Steven R Cranmer, and John C Raymond. Ultraviolet spectroscopy of the extended solar corona. *The Astronomy and Astrophysics Review*, 13(1):31–157, 2006.

[34] RA Kopp and GW Pneuman. Magnetic reconnection in the corona and the loop prominence phenomenon. *Solar Physics*, 50(1):85–98, 1976.

[35] Robert J Leamon, Charles W Smith, Norman F Ness, and Hung K Wong. Dissipation range dynamics: Kinetic alfvén waves and the importance of β e. *Journal of Geophysical Research: Space Physics*, 104(A10):22331–22344, 1999.

[36] Egil Leer, Thomas E Holzer, and Tor Flå. Acceleration of the solar wind. *Space Science Reviews*, 33(1):161–200, 1982.

[37] Xing Li, Shadia Rifai Habbal, John L Kohl, and Giancarlo Noci. The effect of temperature anisotropy on observations of doppler dimming and pumping in the inner corona. *The Astrophysical Journal*, 501(1):L133, 1998.

[38] Benjamin T MacBride, Charles W Smith, and Miriam A Forman. The turbulent cascade at 1 au: energy transfer and the third-order scaling for mhd. *The Astrophysical Journal*, 679(2):1644, 2008.

[39] R Marino, L Sorriso-Valvo, V Carbone, A Noullez, R Bruno, and B Bavassano. Heating the solar wind by a magnetohydrodynamic turbulent energy cascade. *The Astrophysical Journal*, 677(1):L71, 2008.

[40] E Marsch, K-H Mühlhäuser, R Schwenn, H Rosenbauer, W Pilipp, and FM Neubauer. Solar wind protons: Three-dimensional velocity distributions and derived plasma parameters measured between 0.3 and 1 au. *Journal of Geophysical Research: Space Physics*, 87(A1):52–72, 1982.

[41] Eckart Marsch. Radial evolution of ion distribution functions. In Neugebauer [49], pages 355–369.

[42] Lorenzo Matteini, Simone Landi, Petr Hellinger, Filippo Pantellini, Milan Maksimovic, Marco Velli, Bruce E Goldstein, and Eckart Marsch. Evolution of the solar wind proton temperature anisotropy from 0.3 to 2.5 au. *Geophysical Research Letters*, 34(20), 2007.

[43] William H Matthaeus, Gary P Zank, Charles W Smith, and Sean Oughton. Turbulence, spatial transport, and heating of the solar wind. *Physical review letters*, 82(17):3444, 1999.

[44] DJ McComas, M Velli, WS Lewis, LW Acton, M Balat-Pichelin, V Bothmer, RB Dirling Jr, WC Feldman, G Gloeckler, SR Habbal, et al. Understanding coronal heating and solar wind acceleration: Case for in situ near-sun measurements. *Reviews of Geophysics*, 45(1), 2007.

[45] RWP McWhirter and R Wilson. A discussion on the physics of the solar atmosphere-the energy and pressure balance in the corona. *Philosophical Transactions of the Royal Society of London. Series A, Mathematical and Physical Sciences*, 281(1304):331–337, 1976.

[46] Michel Moncuquet, Nicole Meyer-Vernet, Karine Issautier, Marc Pulupa, JW Bonnell, Stuart D Bale, Thierry Dudok de Wit, Keith Goetz, Léa Griton, Peter R Harvey, et al. First in situ measurements of electron density and temperature from quasi-thermal noise spectroscopy with parker solar probe/fields. *The Astrophysical Journal Supplement Series*, 246(2):44, 2020.

[47] Steven Nerney and Aaron Barnes. A reexamination of two-fluid solar wind models. *Journal of Geophysical Research*, 82(22):3213–3222, 1977.

[48] Marcia Neugebauer. Measurements of the properties of solar wind plasma relevant to studies of its coronal sources. In H. Grünwaldt W.K.H Schmidt, editor, *The Source Region of the Solar Wind*, pages 127–151. D. Reidel Publishing Company, 1981.

[49] Marcia Neugebauer, editor. *NASA Conference Publication 2280*, Woodstock, Vermont, 1982.

[50] Marcia Neugebauer and Conway W Snyder. Mariner 2 observations of the solar wind: 1. average properties. *Journal of Geophysical Research*, 71(19):4469–4484, 1966.

[51] Marcia Neugebauer and Conway W Snyder. Mariner 2 observations of the solar wind: 2. relation of plasma properties to the magnetic field. *Journal of Geophysical Research*, 72(7):1823–1828, 1967.

[52] Eugene Parker. Mass ejection and a brief history of the solar wind concept. In Mark Giampapa Jack Jokipii, Charles Sonett, editor, *Cosmic Rays and the Heliosphere*, chapter 1, pages 3–27. The University of Arizona Press, 1997.

[53] Eugene N Parker. Dynamics of the interplanetary gas and magnetic fields. *The Astrophysical Journal*, 128:664, 1958.

[54] Jean C Perez, Sofiane Bourouaine, Christopher HK Chen, and Nour E Raouafi. Applicability of taylor's hypothesis during parker solar probe perihelia. *Astronomy & Astrophysics*, 650:A22, 2021.

[55] JL Phillips and JT Gosling. Radial evolution of solar wind thermal electron distributions due to expansion and collisions. *Journal of Geophysical Research: Space Physics*, 95(A4):4217–4228, 1990.

[56] WG Pilipp, H Miggenrieder, K-H Mühläuser, H Rosenbauer, and R Schwenn. Large-scale variations of thermal electron parameters in the solar wind between 0.3 and 1 au. *Journal of Geophysical Research: Space Physics*, 95(A5):6305–6329, 1990.

[57] John D Richardson and Charles W Smith. The radial temperature profile of the solar wind. *Geophysical research letters*, 30(5), 2003.

[58] Ornulf Sandbaek and Egil Leer. Coronal heating and solar wind energy balance. *The Astrophysical Journal*, 454:486, 1995.

[59] F Scherb. Velocity distributions of the interplanetary plasma detected by explorer 10. *NASA Conf. Publ.*, 1964.

[60] Steven J Schwartz and Eckart Marsch. The radial evolution of a single solar wind plasma parcel. *Journal of Geophysical Research: Space Physics*, 88(A12):9919–9932, 1983.

[61] Rainer Schwenn. The "average" solar wind in the inner heliosphere: Structures and slow variations. In Neugebauer [49], pages 489–509.

[62] Earl E Scime, Samuel J Bame, William C Feldman, S Peter Gary, John L Phillips, and Andre Balogh. Regulation of the solar wind electron heat flux from 1 to 5 au: Ulysses observations. *Journal of Geophysical Research: Space Physics*, 99(A12):23401–23410, 1994.

[63] Jack D Scudder and Stanislaw Olbert. A theory of local and global processes which affect solar wind electrons, 1. the origin of typical 1 au velocity distribution functions—steady state theory. *Journal of Geophysical Research: Space Physics*, 84(A6):2755–2772, 1979.

[64] Charles W Smith, William H Matthaeus, Gary P Zank, Norman F Ness, Sean Oughton, and John D Richardson. Heating of the low-latitude solar wind by dissipation of turbulent magnetic fluctuations. *Journal of Geophysical Research: Space Physics*, 106(A5):8253–8272, 2001.

[65] Joshua E Stawarz, Charles W Smith, Bernard J Vasquez, Miriam A Forman, and Benjamin T MacBride. The turbulent cascade and proton heating in the solar wind at 1 au. *The Astrophysical Journal*, 697(2):1119, 2009.

[66] RS Steinolfson and E Tandberg-Hanssen. Thermally conductive flows in coronal holes. *Solar Physics*, 55(1):99–109, 1977.

[67] Chuan-yi Tu. The damping of interplanetary alfvénic fluctuations and the heating of the solar wind. *Journal of Geophysical Research: Space Physics*, 93(A1):7–20, 1988.

[68] Bernard J Vasquez, Charles W Smith, Kathleen Hamilton, Benjamin T MacBride, and Robert J Leamon. Evaluation of the turbulent energy cascade rates from the upper inertial range in the solar wind at 1 au. *Journal of Geophysical Research: Space Physics*, 112(A7), 2007.

[69] MK Verma, DA Roberts, and ML Goldstein. Turbulent heating and temperature evolution in the solar wind plasma. *Journal of Geophysical Research: Space Physics*, 100(A10):19839–19850, 1995.

[70] Phyllis L Whittlesey, Davin E Larson, Justin C Kasper, Jasper Halekas, Mamuda Abatcha, Robert Abiad, Matthieu Berthomier, AW Case, Jianxin Chen, David W Curtis, et al. The solar probe analyzers—electrons on the parker solar probe. *The Astrophysical Journal Supplement Series*, 246(2):74, 2020.